DTIC

LOCAL CRYSTAL FIELD ANALYSIS OF Eu^{3+} AND Er^{3+} IONS IN A WIDE BAND GAP SEMI-CONDUCTOR GaN.

FINAL TECHNICAL REPORT

BY

PI F. PELLÉ

(MARCH, 2003)

UNITED STATE ARMY

EUROPEAN RESAEARCH OFFICE OF THE U.S. ARMY

LONDON, ENGLAND

R&D Number: 9230-EE-01

CONTRACT NUMBER : N 62558 – 02 –M - 5113

Centre National de la Recherche Scientifique

France

F. PELLÉ

REPORT DOCUMENTATION PAGE

Form Approved OMB No. 074-0188

1. AGENCY USE ONLY (Leave blank)	2. REPORT DATE	3. REPORT TYPE AND DATES COVERED
	March, 2003	Final report

4. TITLE AND SUBTITLE

Local crystal field analysis of Eu^{3+} and Er^{3+} ions in a wide band gap semi-conductor GaN. Contract N62558-02-M-5113

5. FUNDING NUMBERS

W90C2K-9230-EE01

6. AUTHOR(S)

Dr Fabienne Pellé

7. PERFORMING ORGANIZATION NAME(S) AND ADDRESS(ES)

UMR 7574_ Matériaux Inorganiques
Centre National de la Recherche Scientifique
1, Place Aristide Briand
F- 92195 Meudon cedex

8. PERFORMING ORGANIZATION REPORT NUMBER

OWGV1-02-01

9. SPONSORING / MONITORING AGENCY NAME(S) AND ADDRESS(ES)

U.S.Government
US Naval Regional Contracting Center, Detachment London
Government Buildings, Block 2, Wing 12
Lime Grove, Ruislip, Middlesex HA4 8BX
United Kindom

10. SPONSORING / MONITORING AGENCY REPORT NUMBER

11. SUPPLEMENTARY NOTES

12a. DISTRIBUTION / AVAILABILITY STATEMENT

DISTRIBUTION STATEMENT A
Approved for Public Release
Distribution Unlimited

12b. DISTRIBUTION CODE

From time resolved and site-selective excitation spectroscopy, three sites have been identified for Er^{3+} ions in GaN. The main center was ascribed to Er^{3+} ions substituted on the Ga sub-lattice, the two others assigned to Er^{3+} complexes in interstitial positions. The complex decay profile of the $^4S_{3/2}$ fluorescence of the main center and its concentration dependence indicate the occurrence of energy transfers between adjacent Er^{3+} ions. The fluorescent transients were modeled using a diffusion-limited model and the microscopic parameters of the interaction determined. The processes involved in the filling of the infrared emitting level have been identified and suggest a strong interaction between Er^{3+} in interstitial positions and defects nearby. The quenching of the infrared luminescence of the main center is due to a similar diffusion-limited process. The quantum efficiency (QE) of the infrared emission was evaluated and its reduction explained by interaction with free carriers. The crystal field parameter calculated for the main center confirms the substitution of the rare earth in the semiconductor phase excluding oxygen environment. This is supported by the covalent character of the bounding of Er^{3+} to nitrogen in GaN. Three sites were also found for Eu^{3+} ions in GaN. The energy of the Stark components of several levels were determined. The very low energy values compared to that obtained in insulators confirm the strong nephelauxetic effect in GaN due to covalent bonding RE-N. From the scalar crystal field parameter, one Eu^{3+} center has been related to the Er^{3+} main center.

14. SUBJECT TERMS

Section: 4/8 Electronics/Physics
Subsection C : Optoelectronics

15. NUMBER OF PAGES

16. PRICE CODE

17. SECURITY CLASSIFICATION OF REPORT	18. SECURITY CLASSIFICATION OF THIS PAGE	19. SECURITY CLASSIFICATION OF ABSTRACT	20. LIMITATION OF ABSTRACT

KEYWORDS

Optical properties of rare earth ions, crystal field, wide gap semiconductors

TABLE OF CONTENTS

LIST OF ANNEXES

Historical background and motivation of the study

The introduction of Rare Earth (RE) ions as doping in semiconductors has been a challenge for many years. Until recently, most of the studies were investigated for low energy gap systems since the main application was infrared sources for optical communications. However, due to chemical problems, semiconductor hosts cannot accept RE ions with a high concentration. Several attempts were performed in order to increase the solubility of the rare earth in these materials and it has been demonstrated the effect of oxygen impurities which helps to the introduction of the RE in the host. Most of spectroscopic studies have been performed on Er and Yb in small gap semiconductors such as GaAs, InP.

Rare earth (RE) doped wide gap semiconductors have recently appear as a promising new class of materials with potential applications in the field of optoelectronic and photonic. On the other hand, recent use of nonequilibrium growth techniques (ion implantation or thin-film deposition by Molecular Beam Epitaxy or Metallorganic Chemical Vapor Deposition) allows to increase the solubility threshold of the RE in such materials and to dope the semiconductor with concentrations as high as at least 10^{21} cm^{-3}. This opens the opportunity to realize devices for photonic applications. Electroluminescent diodes based on RE^{3+} doped GaN have recently been reported. Emission of the three primary colors has been accomplished using Eu^{3+} for the red, Er^{3+} for the green and Tm^{3+} for the blue lights. Up to now, few studies on RE visible optical properties in such materials have been reported. No clear correlation between the efficiency of the visible RE^{3+} luminescence and the interaction of the rare earth ion with the semiconductor host has been established, especially concerning the RE excitation and deactivation pathways. A full understanding of the properties of the rare earth dopants in the semiconductors and their relationship to growth processes is still incomplete. The aim of this contract was to analyze the local crystal field of Er^{3+} ands Eu^{3+} ions in GaN and to get absolute measurement of the Er^{3+} luminescence efficiency.

The main work has been performed on Er:GaN samples provided by US Labs through ARO since Eu:GaN ones have been available only recently.

I. Er doped GaN

1. Emission spectra

Experimental results are detailed in Annex A. Under excitation below the band gap, the fluorescence spectrum is dominated by the green emission arising from the $^2H_{11/2}$ and $^4S_{3/2}$ multiplets. Radiative transitions are also observed from lower multiplet ($^4F_{9/2}$, $^4I_{9/2}$) with a very weak intensity while infrared emission from $^4I_{13/2}$ exhibits a rather high quantum efficiency compared to previous ones. This indicates that the multiphonon relaxation process is not the main excitation pathway for the $^4I_{13/2}$ multiplet since its probability decreases as an exponential function of the number of phonons required to bridge the energy gap between the optically excited level and the lower one. Lowering the temperature allows to suppress the broadening of the lines due to the spontaneous emission of phonons and several important points should be underlined:

- The emission spectrum, in the visible range, is unchanged (no significant changes in relative intensity, linewidth and wavelength of the different emission lines) when increasing the concentration of Er^{3+} ions. This means that the environment of Er^{3+} remains the same and no other centers are observed with increasing the concentration.
- The infrared emission can be recorded with a quite good efficiency although multiphonon relaxation is almost completely suppressed at low temperature.
- The fluorescence intensity of the visible and infrared emission exhibits a common behavior with the Er^{3+} concentration. It increases with the concentration up to a maximum (0.6 at.%) and then

decreases. The reduction of the fluorescence intensity is assigned to interactions between nearby Er^{3+} ions leading to other de-excitation pathways.

- The energies of the Stark components and the overall splitting of the multiplets are very similar to that observed in insulators.

Two questions arise from these remarks: what is the main excitation process for populating the infrared emitting level? what is the nature of the process leading to the quenching of the luminescence? To answer these questions, site selective excitation spectroscopy and the time dependence of the visible and infrared fluorescence have been investigated.

2. Site selective excitation spectroscopy

Selective excitation spectrum has been analyzed, at low temperature (T=10K), monitoring the $^4I_{13/2} \rightarrow {}^4I_{15/2}$ four main emission lines. The most intense lines are only excited in the $^2H_{11/2}$ state. Excitation spectra of the two weaker lines are more complex, a weak excitation is observed when excitation is in resonance with the $^2H_{11/2}$ state while another efficient excitation peak is observed at a wavelength which depends on the analysis. It is important to note that these latter lines fall off-resonance with absorption of 4f -intra shell transitions.

Selective excitation in the different excitation lines gives rise to three different infrared spectra which are ascribed to different emitting centers. The different centers will be labeled, in the following, as C1, C2 and C3 for simplicity. Selective excitation in both lines out of resonance with Er^{3+} levels provides emission intensity one order of magnitude higher than in the intra-4f configuration and the emission spectrum strongly depends on the excitation wavelength. With increasing the temperature, C2 and C3 fluorescence decreases greatly and cannot be recorded.

Excitation of the $^4I_{13/2}$ multiplet below the band gap and out of the absorption range of the $Er^{3+}(^{2S+1}L_J)$ states of the 4f configuration has already been reported in Er-implanted GaN/Al_2O_3 thin films [(1)]. In this case, the excitation spectrum consists of an unstructured broad band extending from 460 to 530 nm. This result is not completely in agreement to ours since we observe a $^4I_{13/2} \rightarrow {}^4I_{15/2}$ emission which depends on the excitation wavelength and which excitation spectrum consists in narrow lines. However, the energy of these extra excitation lines is well in the range of the broad excitation band. Furthermore, the shape of the emission spectra of C2 and C3 are very similar to that observed in ref. (1). In both cases, the luminescence intensity provided by extra 4f-intraconfigurational excitations is one order of magnitude more intense than that recorded with a resonant 4f-4f excitation. Due to the strong efficiency of these extra excitations, and to the fact that the intra-4f transitions have very low absorption cross sections ($\approx 10^{-6}$) compared to that of excitons ($\approx$0.01-1), this suggests that excitation of C2 and C3 centers does not proceed via Er^{3+} 4f-4f intra-shell transitions but rather by an Er^{3+}-trap-related absorption line. In addition, no emission in the visible or in the infrared can be recorded for these centers with direct excitation in their 4f configuration. So, despite a lower intensity in the infrared for C1, this center can be directly excited in the 4f-intrashell transitions which oscillator strengths are very weak. Furthermore, as it will be reported in the following, the complex behavior of the visible decay profile suggests interactions between Er^{3+} in center C1 resulting from clustering of the RE in the sample. For these reasons we conclude that C2 and C3 concentrations are much lower than that of C1.

From the considerations above, the X-rays diffraction spectra as a function of the Er^{3+} content, C1 center corresponds to Er^{3+} ions in regular positions in the lattice. Moreover, from Rutherford Back Scattering channeling analysis, it has been shown in the studied samples that a great majority ($\approx$95 %) of the Er^{3+} ions occupy sites on the Ga sublattice even at relatively high concentration [(2)]. Most of the doping ions substitute on Ga sites. The Solid Source Molecular Beam Epitaxy growth method allows to introduce RE ions with high concentration, however they form clusters even at low concentration as it is observed by the strong quenching of the luminescence. For higher Er^{3+} content, a pure ErN phase is

obtained as shown by X-rays diffraction demonstrating the clustering of Er^{3+} in the GaN host [3]. C2 and C3 centers could be ascribed to Er^{3+} ions in interstitial positions near defects produced by either introduction in the lattice, as it is observed in other RE doped semiconductors. The difference of the shape (broad band versus narrow lines) recorded for Er –trap related defects can be explained by considering the growing process used in (1) and in the present work. The implantation doping is a simple method and the doping level can be controlled independently of the growing conditions, however, this method provides introduction of damage in the GaN which cannot be completely removed by annealing. So a higher concentration of defects or the presence of extended defects are expected in the implanted samples, this may be explain the observation of a broad band compared to our samples, obtained by MBE, in which the defects should be more localized then giving rise to a discrete spectrum.

3. Time resolved spectroscopy

3.1. Visible emission

Since emission from C1 and C2 centers are not observed in the visible range, this part concerns the dynamic of the C1 center which will be considered as the main one. The mean lifetime is strongly reduced compared to that is obtained usually for the $^4S_{3/2}$ state even after correction due to the local field related to the high index of refraction of GaN. Several competing processes have to be considered which induce a shortening of the decay of the $^4S_{3/2}$ multiplet (radiative de-excitation, multiphonon relaxation, diffusion, energy transfers). As we have previously shown the quite efficient emission from the $^4I_{13/2}$ level compared to that of the intermediate states ($^4F_{9/2}$ and $^4I_{11/2}$) indicates that the multiphonon relaxation is not the main process involved in the de-excitation process of the optically excited state. The time development of the $^4S_{3/2} \rightarrow {}^4I_{15/2}$ fluorescence intensity at room temperature deviates from a simple exponential dependence whatever the Er^{3+} concentration from 0.025 to 11.2 at.%. From the evolution of the decay profile with the Er^{3+} concentration (increasing of the deviation of the initial part of the decay from a simple exponential law ; the long part of the decay, following an exponential behavior, remains nearly the same for low Er^{3+} concentrations and gradually increases with the Er^{3+} content), then ion-ion interactions should be taken into account to explain the profile and the strong reduction of the observed decay.

To determine the processes involved in the non-radiative energy transfer we will consider a set of Er^{3+} ions acting as "sensitizers" and the other set being the "acceptors" which trap the energy and produce the quenching of the luminescence of the sensitizers; the acceptors could be other Er^{3+} ions or sinks such as "poisonous centers", the last kind is very often evoked but until now no nobody could give a proof of their real nature. So, in the following we will consider that Er^{3+} ions as sensitizers and activators which is a more realistic hypothesis. The complex time development of the intensity of the sensitizers results from direct energy transfer and energy migration to acceptors and three limiting cases can help to describe the relaxation of the sensitizer sub- system: fast diffusion, direct relaxation – no diffusion and diffusion-limited relaxation. The behavior of the sensitizer fluorescence transient as a function of the acceptor concentration had allowed us to characterize the sensitizer-sensitizer and sensitizer-acceptor dynamics and helps to identify the dominant mechanism involved in the sensitizer luminescence quenching process. According to our experimental results, the decay curves had been modeled in the limited-diffusion case and the sensitizer-acceptor interaction was found to be dipole-dipole type. The diffusion-limited model is detailed in Annex B. All the microscopic parameters which characterize the Er^{3+}-Er^{3+} interaction and the diffusion constant, in the different GaN samples, have been determined. The theoretical curves calculated with the complete expression for a diffusion-limited process are in complete agreement with all the experimental decay curves.

Measured values of the diffusion constant for rare earth ions in insulators range from 10^{-11} cm^2 s^{-1} to $10^{-9}cm^2$ s^{-1}, many orders of magnitude smaller than for excitons in molecular crystals [4]. Up to now very few studies on the spectroscopy of rare earth in semiconductors and especially on their interaction

with free carriers have been reported to explain the spectroscopic properties observed in the visible spectral region. Further experiments are needed, in the future, to explain such high values for the diffusion constant calculated for Er:GaN.

3.2. Infrared emission

In this case, the temporal behavior of the $^4I_{13/2}$ state has been studied at low temperature for the different centers and as a function of the Er^{3+} concentration for the main center at room temperature.

3.2.1. Main center : Time resolved emission spectrum

Time resolved emission spectrum from $^4I_{13/2}$ to the ground state for center C1, recorded at 10K with excitation in the $^2H_{11/2}$ multiplet, exhibits several features which behave in the same way as the delay increases. This confirms that all of them belong to the same center, C1. On the other hand, the spectrum recorded at a long delay after the pulse excitation reveals a reabsorption of the resonant fluorescence which is ascribed to a radiative energy transfer which gives an additional contribution to migration within the $^4I_{13/2}$ state. The quenching of the $^4I_{13/2}$ will be discussed in the following.

3.2.2. Dynamic of the infrared emission

The decay of the $^4I_{13/2}$ state has been measured at low temperature for the different centers. The excitation pathway for center 1 is found completely different from others. C1 exhibits a long rise time of the fluorescence. From the complex decay behavior observed for the visible emission, the quasi-absence of emission from intermediate states between the excited level and the emitting one, we can suggest that the process involved for the population of the $^4I_{13/2}$ state of C1 center is due to a cross relaxation process $(^4S_{3/2},^4I_{15/2})\rightarrow(^4I_{11/2},^4I_{13/2})$ after migration of the excitation within the $^4S_{3/2}$ state as we have demonstrated the occurrence. The $^4I_{13/2}$ state is then populated through mainly the $^4I_{11/2} \rightarrow {}^4I_{13/2}$ radiative transition. The rise time observed is easily ascribed to the $^4I_{11/2}$ lifetime since at 10K multiphonon process probability is very low and 6 phonons, assuming a phonon cut-off frequency of 600 cm^{-1} as deduced by vibrational spectroscopy are required to bridge the energy gap between those two levels. The value then obtained for low Er^{3+} concentrations is quite in agreement with values measured for this level in other lattices.

In case of C2 and C3 centers, the process populating the emitting level is faster and we propose a population through a similar cross relaxation process between the related trap excited level and the $^4I_{13/2}(Er^{3+})$ one, this process can explain why no emission from the $^4S_{3/2}$ level can be observed for these centers. In addition, C2 and C3 exhibit quite similar time constants (rise and decay times) which means that they correspond to Er^{3+} ions in a quite similar environment.

The fluorescence transients of the $^4I_{13/2}$ state for center C1 has been measured as a function of the Er^{3+} concentration. All time constants are strongly reduced with increasing the Er^{3+} content in the samples. The reduction of the time constants and the observation of the radiative trapping of the infrared emission are a sign of Er^{3+} - Er^{3+} interactions also in the $^4I_{13/2}$ state.

3.2.3. Main center : self-quenching of the infrared emitting level

Although the quenching process cannot any longer be attributed to a cross-relaxation step as for $^4S_{3/2}$, the self-quenching behavior is still well described by a limited-diffusion process. The $^4I_{13/2}$ state, being the first excited state, no cross-relaxation is likely to occur and diffusion towards quenching centers has to be looked for to explain the concentration dependence of the lifetime. Since a diffusion-limited process is observed as for $^4S_{3/2}$, efficient quenching centers are operative. *A priori*, in absence, of RE impurities with lower energy levels such as Ho^{3+}, Tm^{3+}, Dy^{3+}... ; the quenching centers can be readily attributed to centers C2 and C3 which have levels at slightly lower energy and shorter lifetimes. The comparison between the critical concentrations calculated for both levels, ($4.31\ 10^{21}$ cm^{-3} for $^4S_{3/2}$ versus $0.67\ 10^{21}$ cm^{-3} for $^4I_{13/2}$) indicates that the Er^{3+} first excited state is unusually more self-quenched than the higher lying level.

If quenching centers are C2 and C3 which are ascribed to Er^{3+} ions in interstitial position, self-quenching at 1.5 μm could be reduced by reducing the instertitial ion number at higher Er^{3+} concentration. The introduction of the RE in interstitial position is most probably caused by the large ionic radii differences between Ga and RE ions (0.62 Å against 1 Å). A small replacement of Ga by In (0.85 Å) could help the introduction of Er^{3+} ions on Ga positions.

3.2.4. Quantum efficiency of the infrared emission

The lifetime measured at low temperature compared to that obtained at room temperature for a weakly concentrated sample indicates that a thermal process is taking place at room temperature. Due to the large energy gap between the $^4I_{13/2}$ state and the next lower state i.e. the ground state, the multiphonon process is not efficient and the role of free carriers could be recognized here. We have attempted to evaluate the radiative lifetime from the lifetime measured at low temperature for a low concentrated sample.

For rare earth ions in semiconductors, it has been demonstrated that the matrix elements for radiative transitions are not very different from the ones in insulators hosts. Then, we expect that the radiative lifetime should be the same for the same index of refraction (since the local field is the most important parameter for the radiative rate) and assuming a similar crystal field strength. Under these considerations, the $^4I_{13/2}$ radiative lifetime in GaN can be estimated by comparison with the result obtained in a fluoride glass which exhibits a relatively weak crystal field as GaN (the crystal field strength is calculated in the following). In the fluoride glass, due to a low phonon cut-off frequency, the measured lifetime (9 ms) corresponds to the radiative lifetime calculated by application of the Judd-Ofelt theory [5]. From this, the radiative lifetime for Er in GaN is estimated to be:

$$\tau_{RGaN}=\tau_{RFluor}(n_{Fluor})^2/(n_{GaN})^2\cong 4 \text{ ms}$$

where the refractive index $n_{Fluor}=1.5$, n_{GaN} is taken as 2.25 at 1.54 μm.

This result shows that even at low temperature and weak concentration the quantum efficiency for the 1.5μm emission is τ_0/τ_R, limited to about 3.1/4=77% and to 2.5/4=62.5% at low and room temperature respectively. The phonon cut-off frequency being of the same order to that of the fluoride glass, the energy transfer to free carriers could explain that quantum efficiency in lower in GaN than in an insulator. In order to ascertain this point, a more precise determination of the radiative lifetime would be necessary through an absolute determination of the transition oscillator strength. This point was supposed to be done in this contract but unfortunately, due to the very weak oscillator strength of the 4f-4f transitions, the depletion of the beam by absorption is too weak to allow absorption coefficient measurements. The knowledge of the carrier concentration at various temperatures would be also useful.

4. Crystal field analysis

Elements of theory concerning this section are reported in Annex C.

4.1. Crystal field strength

From the emission spectrum recorded for different excited states of C1, the energies of the Stark components and then overall splitting of the ground state could be deduced. From the energy level scheme, it is possible to evaluate the crystal field strength of GaN and to compare it with other materials such as insulators in which RE optical properties are widely developed. Such a comparison should allow to deduce if Er^{3+} ions are really embedded in the semiconductor host or linked to oxygen ions as it is often observed, a good example is given by the Er in GaAs were the strong luminescence efficiency has been related to the Er-2O center [6].

The degeneracy of a $4f^N$ multiplet is removed by the crystal field and the energy of the resulting Stark components are expressed in terms of crystal field parameters which number depends on the site symmetry. As an example, for low site symmetry, 15 different parameters are needed to describe the crystal field effect on the Stark levels. This prevents a simple comparison of the crystal field strength between several hosts. The scalar crystal field parameter N_v was introduced to allow a simple comparison between different host materials [7]. The maximum splitting $\Delta E(J)$ for a J given state of a rare earth ion in a crystal is simply related to the crystal field strength parameter N_v, for the multiplets of interest in this work following relations are obtained :

$$\Delta E(15/2) = 0.192\ N_V$$
$$\Delta E(13/2) = 0.117\ N_V$$

From the experimental results, the energies of the Stark components of the $^4I_{15/2}$ multiplet were deduced. The overall splitting, $\Delta E(^4I_{15/2})$, of the $^4I_{15/2}$ multiplet was found equal to 299 cm^{-1}. The scalar crystal field strength parameter, N_v, is found equal 1557 cm^{-1}.

The scalar crystal field parameter can also be used to calculate the maximum splitting of the other multiplets of Er^{3+}. Using the relation given above and the calculated value for N_v, the overall splitting of the $^4I_{13/2}$ multiplet was evaluated as 182 cm^{-1}. The splitting, measured for the $^4I_{15/2}$ ground multiplet and calculated for the first excited $^4I_{13/2}$ multiplet, compared to experimental values reported in literature for several inorganic materials [6,8,9], allows to classify GaN as a weak field material. From a general point of view, halides correspond to weak field materials while oxides exhibit strong crystal field. From the N_v value evaluated for the Er^{3+} doped GaN, it is possible to evaluate the crystal field strength expected for Nd^{3+} doped GaN by talking into account for the lanthanide contraction [10]. This gives $N_v(Nd^{3+})$ equal to 2139 cm^{-1} which is between those obtained for $LaCl_3$ (1062 cm^{-1}) and LaF_3 (2356 cm^{-1}). This result confirms that the crystal field strength in GaN is much weaker than in oxides for which the N_v value has been found to be larger than 3000 cm^{-1} [11]. This indicates that the rare earth is well imbedded in the semiconductor host and not in an oxide impurity phase.

On the other hand, comparing the results obtained for Er^{3+} in GaN (this work) and in GaAs [6], the overall splitting for $^4I_{13/2}$ (353 cm^{-1}) in GaAs would give a much higher N_v value (2504 cm^{-1}) in agreement with an oxygen surrounding [6]. Since the N_v value of 1557 cm^{-1} found for GaN is clearly lower than that obtained for GaAs or the oxide hosts, our results point to the replacement of Ga by the rare earth in the semiconducting phase.

4.1. Nephelauxetic effect

Another way to verify this hypothesis is to study the nephelauxetic red shift [12] of the $^4I_{13/2}$-$^4I_{15/2}$ transition barycenter at 1.5 μm for various Er^{3+} doped hosts. These can be calculated from the experimental results given in literature [6,8,9]. The barycenter value found for GaN is between the value for YAG and $CsCdBr_3$ clearly shows a covalent surrounding for Er^{3+} ions in the semiconductor host.

Comparing with the results obtained for the Er-2O center in GaAs which exhibits a strong crystal field, the main center C_1 in GaN shows a typical behavior which could be expected for a Ga site with covalent bonding to nitrogen: a weak crystal field and a large nephelauxetic red shift.

II. Eu^{3+} doped GaN

Among lanthanide trivalent ions, trivalent europium, Eu^{3+}, exhibits the simplest energy level scheme in the visible range. Moreover, the main emitting level, $^5D_0$, being non degenerate the luminescence spectrum is easy to interpret and therefore the Eu^{3+} ion has been widely used as a local probe. The spectroscopic study of the Eu^{3+} ions in GaN was performed in order to get more detailed information about the nature of the two extra centers found for Er^{3+} doped GaN, while the final aim was to evaluate the crystal field effect in GaN.

This part of the final report will be more detailed since the results have not been reported in earlier reports. Figures are reported in annex D.

1. Crystal field components and selection rules for electronic multipole transitions

From Rutherford Back Scattering analysis, the Eu^{3+} ions in GaN occupy a site of C_{3v} point symmetry. This introduces further simplifications in the interpretation of the luminescence spectra since the degeneracy of the $^{2S+1}L_J$ states is not completely lifted due to the symmetry and the number of observed transitions is reduced. The number and symmetry labels of the crystal field components of the ^7F_J levels for the C_{3v} point symmetry are reported in Table 1-Annex D.

The transitions between the free ion levels of Eu^{3+} have a multipolar character. In addition to the electric dipole induced transitions, a few magnetic dipole transitions with a non-negligible transition probability are observed for Eu^{3+}. The selection rule for the magnetic dipole transitions is $\Delta J = 0, \pm 1$, with $0 \leftrightarrow 0$ forbidden. If the mixing of states with different J values is disregarded, the selection rule for electric dipole transitions gives $\Delta J \leq 6$ and, in the special case of the initial or final level having a J value equal to zero, one obtains $\Delta J = 2,4,6$.

The crystal field operator authorizes the mixing of states with different J values thus rendering the group theoretical selection rules as the only valid ones. These rules obtained for the C_{3v} site symmetry are gathered in Table 2 – Annex D together with the appropriate polarization of the emission lines.

2. Experimental results

2.1. Optical measurements

The study of spectroscopic properties of Eu^{3+} in GaN was performed on three samples (D120,D035 and RJ081), the last one being synthesized by using another different method. Under excitation above the energy gap, at room temperature, the luminescence recorded between 520 and 720 nm is dominated , for each sample, by a red emission which is easily ascribed to the $^5D_0 \rightarrow {}^7F_2$ transition (Figure 1-Annex D). Weak emission lines observed between 530 and 570 nm can be assigned to the radiative transitions arising from the $^5D_1$ state. The emission from the $^5D_{1\text{-}4}$ levels of the Eu^{3+} ion is generally quenched by multiphonon relaxation of the excitation energy. In GaN, the low vibrational energies cause low multiphonon relaxation rates and hence allow the observation of emission from upper multiplets, at least from $^5D_1$ and $^5D_2$. In the case of Eu^{3+}:GaN, it appears from the energy of observed emission lines that the corresponding transitions originate only from $^5D_1$ and $^5D_0$.

Even if the overall luminescence spectra seem similar for each sample, a careful examination of the $^5D_0 \rightarrow {}^7F_2$ transition allows to observe some differences from one sample to another. Roughly the same emission peaks are observed but with different relative intensities as shown on Figure 2-Annex D. The luminescence decay depends on the emission wavelength (Figure 3-Annex D), which indicates a contribution of several sites to the emission. This has already been observed for another kind of the

Eu^{3+}:GaN sample [13]. Figure 2 - Annex D suggests that all centers are present in each sample even if in different concentrations which explains the variation in the intensity of observed lines.

In addition, the luminescence spectrum for the Eu^{3+}:GaN sample D035 recorded at low temperature (10 K) under excitation above the gap is quite different to that recorded at room temperature as shown on Figure 4 – Annex D:

- Between 530 and 570 nm, a strong emission corresponding to the $^5D_1 \rightarrow {}^7F_0$ transition is observed at 533 nm while the $^5D_1 \rightarrow {}^7F_1$ transition is weak. At room temperature, $^5D_1 \rightarrow {}^7F_1$ is quite efficient while no emission is observed for the $^5D_1 \rightarrow {}^7F_0$ transition. No simple physical process can be found to explain this result.
- The $^5D_0 \rightarrow {}^7F_2$ transition is quite different.

From these considerations, we suppose that the dominant emitting centers are not the same at low and room temperature.

2.2. Energies of the crystal field components of the $^{2S+1}L_J$ multiplets

2.2.1. $^5D_1$ and $^5D_0$ levels

In order to determine the energy of the Stark components of the different $^{2S+1}L_J$ multiplets, excitation spectra were measured monitoring the main $^5D_0 \rightarrow {}^7F_2$ transition. The luminescence efficiency is much lower when excited in the 4f-intrashell configuration as shown on the spectrum reported on Figure 5a – Annex D. However, in the range of the $^7F_{0,1} \rightarrow {}^5D_1$ transitions several lines were observed, three for $^7F_0 \rightarrow {}^5D_1$ (noted as * in Figure 5a). Resonant excitation on each of them gives rise to slightly different spectra for the $^5D_0 \rightarrow {}^7F_2$ transitions. This observation prevents to assign these three lines to the transitions from the ground state $^7F_0$ to the three $^5D_1$ Stark components of a $^5D_1$ manifold. Fortunately, it has been demonstrated, by collecting a large number of data, a linear relation between the energies of the different multiplets for a given $4f^n$ configuration [Lella] and in the case which is of interest for us, a linear relation has been established between the barycenter of $^5D_1$ with the energy of $^5D_0$. The energy found for the three $^5D_1 \rightarrow {}^7F_0$ observed transitions reported on the theoretical curve (Figure 6 – Annex D) allows to locate the $^5D_0$ level energy at 17009 (587.9), 16964 (589.5) and 16939 cm^{-1} (590.3 nm) associated with the three observed $^5D_1$ states. Experimentally we observe $^5D_0 \rightarrow {}^7F_0$ emission lines in this spectral range at 585.2, 588.6 and 592.2 nm. These energies are very low compared to those obtained for the inorganic materials considered to establish the curve in Figure 6 and this confirms again the high degree of covalency in the rare earth – nitrogen bonding as was already observed for Er^{3+} doped GaN. The agreement between our experimental results and the curve in Fig. 6 is not perfect because the curve was established for the $^5D_1$ barycenter whereas the value of $^5D_1$ used here in this curve corresponds to only one component. Thus its energy is slightly different from the barycenter energy. Centers associated with each $^5D_0 \rightarrow {}^7F_0$ transition will be labeled as C1 (585.2), C2 (588.6) and C3 (592.2 nm) in the following for the sake of simplicity.

2.2.2. $^7F_1$ level

Due to the overlap of the emission from the $^5D_0$ and $^5D_1$ levels, especially in the range between 590 and 615 nm, the interpretation of the spectrum is not straightforward and requires other investigations in order to separate the transitions coming from the $^5D_1$ multiplet and from $^5D_0$ observed in this range.

First by lowering the temperature, the multiphonon relaxation probability from $^5D_1$ to $^5D_0$ decreases and the transitions arising from $^5D_1$ gain intensity. Excitation above the band gap gives rise to a strong emission at 532.7 nm which is ascribed to the $^5D_1 \rightarrow {}^7F_0$ transition. There is a good agreement between this emission line and one of the $^5D_1 \rightarrow {}^7F_0$ excitation peaks assigned to center C1 as can be seen on Figure 5b - Annex D. Two weak emission lines observed at shorter wavelengths are assigned to the

$^5D_1 \rightarrow {}^7F_1$ transition and allows to determine the energy of the $^7F_1$ Stark components associated to the C1 center.

On the other hand, the $^5D_1$ decay is usually much shorter than that of $^5D_0$ due to the nonradiative relaxation to $^5D_0$. Then recording the emission with different delays after the excitation pulse can help to assign the emission lines from different emitting levels (Figure 7 – Annex D). This experiment was carried out and the lines remaining after the long delay were assigned to the $^5D_0 \rightarrow {}^7F_1$ transitions of the three centers. Considering the results obtained for the different samples, we attempted to define the energies of the $^7F_1$ Stark components for the C2 and C3 centers. Since there exists a linear relation between the $^5D_0$ level energy and the $^7F_1$ barycenter energy, this relation can help to ensure the attribution and to allow to ascribe the relative position of the doubly degenerate level E and non degenerate one (A_2). Our data agree quite well with the theoretical curve which seems to support the validity of our attribution as shown on Figure 8 – Annex D.

2.2.3. $^7F_2$ level

When the resonant excitation was performed on the $^5D_0$ state of the C1 center, the overall emission is very weak and only the $^5D_0 \rightarrow {}^7F_2$ transition could be measured with significant intensity. However, it allows to precise the energy of the $^7F_2$ Stark components for the C1 center. From the decay measurements (Figure 3 – Annex D) it was found that the lifetimes of the $^5D_0$ levels associated to the different centers are of the same order of magnitude. In this case, the Time Resolved Spectroscopy cannot help so much to differentiate the different centers. The energies of the $^7F_2$ components were thus deduced by the mathematical deconvolution analyses of the emission spectra, assuming three components for each center. Best fits are obtained with the Lorentzian profiles for the individual transitions (Figures 9a,9b and 9c – Annex D). The peak energies deduced from the fit remain roughly the same from a sample to another. From these results, it appears that the C1 center is the main emitting level for the Eu^{3+}:GaN sample D035 at low temperature while the C2 and C3 centers are observed at room temperature. The barycenters determined by this way, are in good agreement with the theoretical relation between barycenters of the $^7F_2$ and $^7F_1$ levels as it can be seen on Figure 10. All the experimental level energies are reported in Table 3 as well as in Figures 11 and 12 – Annex D.

3. Crystal field analysis

In the case of a C_{3v} site symmetry, the crystal field splitting of the $^7F_1$ manifold is easy to describe since the energy of the components of the $^7F_1$ multiplet depends only from one crystal field parameter B_0^2:

$$E(E) = E_0(^7F_1) - \frac{B_0^2}{10} \tag{1a}$$

$$E(A_2) = E_0(^7F_1) + \frac{B_0^2}{5} \tag{1b}$$

where $E_0(^7F_1)$ is the energy of the $^7F_1$ state when the second order terms of the crystal field potential are zero.

The B_0^2 parameter, deduced from Eqs. (1a), (1b) and the splitting of $^7F_1$ for each center, shows a strong variation among the three centers as shown on Figure 13. The knowlegde of this parameter allows to evaluate the crystal field strength parameter N_v acting on Eu^{3+} in GaN. It follows from Eq.(2) of Annex C that the $^7F_1$ splitting is related to B_0^2 through the simple expression :

$$N_v = \left[\frac{4\pi}{5}\left(B_0^2\right)^2\right]^{1/2} \tag{2}$$

	ΔE (cm^{-1})	B_0^2 (cm^{-1})	N_v (cm^{-1})
C1 center	92	-307	487
C2 center	129	+430	682
C3 center	291	+972	1541

By taking into account for the lanthanide contraction[10], it has been demonstrated that the crystal field strength parameter for a given $4F^N$ configuration can be obtained from that of Nd^{3+} by using the following relation:

$$N_v(4F^N)=N_V(Nd^{3+})-0.034(N-3)N_v(Nd^{3+}) \quad (3)$$

For the crystal field strength parameter evaluated to 2139 cm^{-1} for Nd^{3+}:GaN, the Eq. (3) gives a value of 1921 cm^{-1} for Eu^{3+}. This value is quite comparable to that obtained experimentally for the C3 center.

As a conclusion to this study, three centers are identified for Eu^{3+} in GaN. From the crystal field considerations, it appears that the C3 center corresponds to the main Eu^{3+}center. The energies of the different levels were found very low compared to the values obtained for insulators. This demonstrates the strong nephelauxetic effect due to the covalent Eu-N bounding.

Conclusion and recommendations

From time resolved measurements and site-selective excitation spectroscopy, three kinds of sites have been identified for the Er^{3+} ions in GaN. The majority of Er^{3+} ions was determined to be substituted on the Ga sub-lattice which is considered as the main center. The two other sites were assigned to Er-related defects and ascribed to Er^{3+} complexes in interstitial positions or in the N sublattice. A non-exponential time behavior for the decay profile was observed for the $^4S_{3/2}$ fluorescence of the main center. The complex decay profile and its concentration dependence indicate that the optical relaxation involves energy transfer processes between adjacent Er^{3+} ions. The fluorescent transients were modeled and interpreted using a diffusion-limited migration of the optical interaction. All the microscopic parameters characterizing the interaction were determined and compared to the experimental data.

The processes involved in the filling of the infrared emitting level have been identified and suggest a strong interaction between Er^{3+} ions in interstitial positions and defects nearby. The quenching of the infrared luminescence recorded for the main center is found to occur due to a similar diffusion-limited process in which acceptors could be identified to other centers ascribed to Er^{3+} in interstitial positions. The quantum efficiency of the infrared emission was evaluated to be 77% and 62.5 % at low and room temperature respectively. The reduction from 100% expected for such energy gap between the emitting level and the next lower one cannot be explained from a multiphonon relaxation process, interaction with free carriers is suggested.

The crystal field parameter calculated for Er^{3+} in the main center compared to that in other inorganic materials confirms the substitution of the rare earth in the semiconductor phase excluding oxygen environment. This is supported by the covalent character of the bounding of Er^{3+} to nitrogen demonstrated for the main center in GaN.

Three sites were also found for Eu^{3+} ions in GaN, their relative concentration appears to be dependent on the Eu^{3+} concentration and on the growing method. In this case, the study of the interaction between ions is not possible since, due to its energy level scheme, Eu^{3+} is much less sensitive to cross-relaxation processes which occur by energy transfer between nearby ions. The energy of the different Stark components of the $^5D_0$, ^7F_J (J=1,2) levels were determined. All these energies were found very low compared to that obtained in insulators. This confirms the strong nephelauxetic effect in GaN due to covalent bonding RE-N. From the scalar crystal field parameter, one Eu^{3+} center seems to be related to the main center observed for the Er doped GaN samples.

This study to be really complete requires other investigations, especially in order to understand :

- The role of the free carriers in the diffusion process.
- The correlation between the concentration of the different centers and the growing process.
- The correlation between Eu and Er centers.

LITERATURE CITED

1. H. Przybylińska, A. Kozanecki, V. Glukhanyuk, W. Jantsch, D.J. As and K. Lischka, *Physica B*, **308**, 34 (2001).
2. K. Lorenz, R. Vianden, R.H. Birkhahn, A.J. Steckl, M.F. Da Silva, J.C. Soares and E. Alves, *Nucl. Instr. Meth. B*, **161/163**, 946 (2000).
3. D.S. Lee, J. Heikenfeld, A.J. Steckl, U. Hömmerich, J.T. Seo, A. Braud and J.M. Zavada, *Appl. Phys. Lett.*, **79**, 719 (2001).
4. R.C. Powell and Z.G. Soos, *J. Lumin.*, **11**, 1 (1975).
5. M.D. Shinn, W. Sibley, M.G. Drexhage and R.N. Brown, *Phys. Rev. B*, **27**, 6635 (1983).
6. H. Hennen, J. Schneider, G. Pomerenke and P.C. Becker, *Appl. Phys. Lett.*, **43**, 943 (1983).
7. F. Auzel and O. Malta, *J. Physique*, **44**, 201 (1983).
8. A. A. Kaminskii, *Laser Crystals : Their physics and properties*, Springer Verlag, Berlin (1990).
9. N.J. Cockroft, G.D. Jones and R.W.G. Syme, *J. Lumin.*, **43**, 275 (1989).
10. F. Auzel, *Opt. Mat.*, **19**, 89 (2002).
11. E. Antic-Fidancev, J. Hölsä, M. Lastusaari and A. Lupei, *Phys. Rev. B*, **64**, 195108 (2001).
12. C.K. Jorgensen, *Prog. Inorg. Chem.*, **4**, 73 (1962).
13. Ei Ei Nyein, U. Hömmerich, J. Heikenfeld, D.S. Lee, A.J. Steckl and J.M. Zavada, *Appl. Phys. Lett.*, **82**, 1655 (2003).
14. E. Antic-Fidancev, J. Alloys and Compounds, 300-301, 2 (2000).

ANNEX A

Spectroscopy of Er^{3+} in GaN

1. Emission spectra

1.1. Visible emission

Figure 1:Visible fluorescence spectrum of GaN: Er^{3+} (0.17 at.%) recorded at room temperature under resonant excitation in the $^4F_{7/2}$ multiplet ($\lambda_{excitation}$= 498 nm).

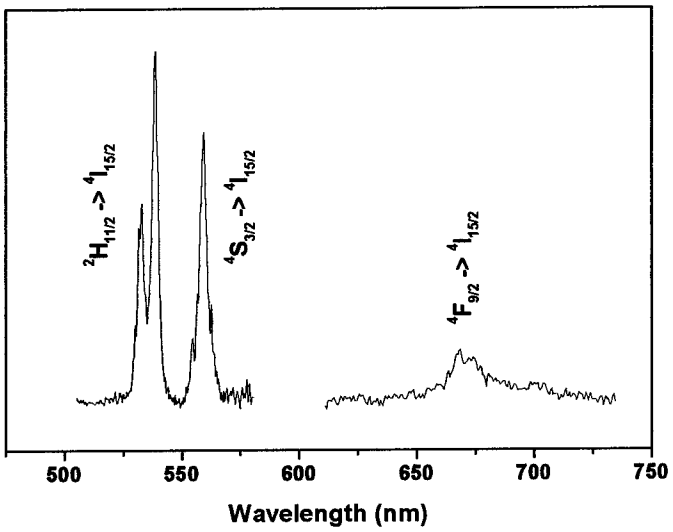

Figure 2 : $^4S_{3/2} \rightarrow {}^4I_{15/2}$ emission spectrum recorded at 10K with excitation in the $^2H_{11/2}$ multiplet (GaN :Er^{3+} 0.17 at.%).

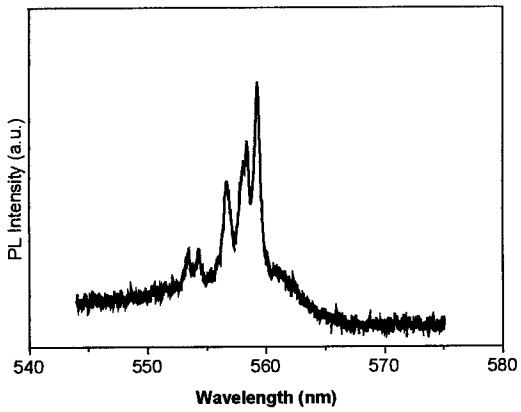

1.2. Infrared emission

Figure 3: : $^4I_{13/2} \rightarrow {}^4I_{15/2}$ emission spectrum recorded at 300 K with excitation in the $^2H_{11/2}$ multiplet (full line :Er^{3+} 0.6 at.% ; dotted line : Er^{3+} 0.17 at.%).

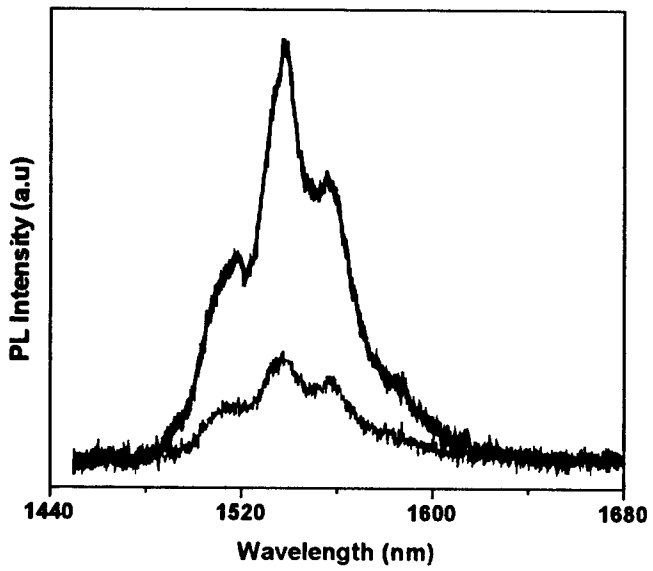

Figure 4: $^4I_{13/2} \rightarrow {}^4I_{15/2}$ Fluorescence spectrum recorded at 10K for GaN :Er^{3+} (0.6 at.%) with excitation in the $^2H_{11/2}$ multiplet.

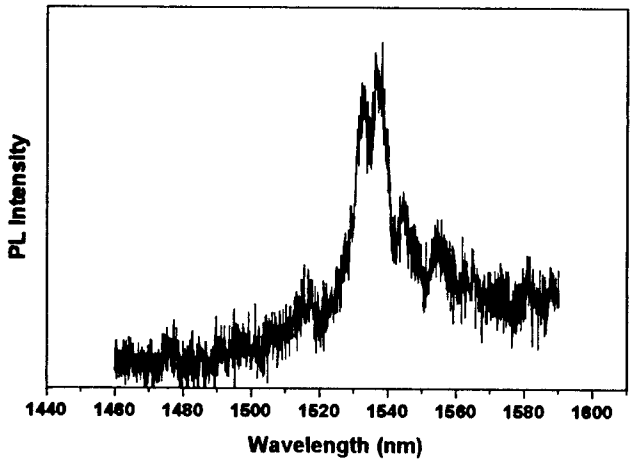

2. Time resolved spectroscopy

2.1 .Visible emission

Figure 5: $^4S_{3/2}$ decay profile as a function of Er^{3+} concentration (T=300K) (Symbols : experimental data ; full lines : theoretical curves calculated using the diffusion-limited model).

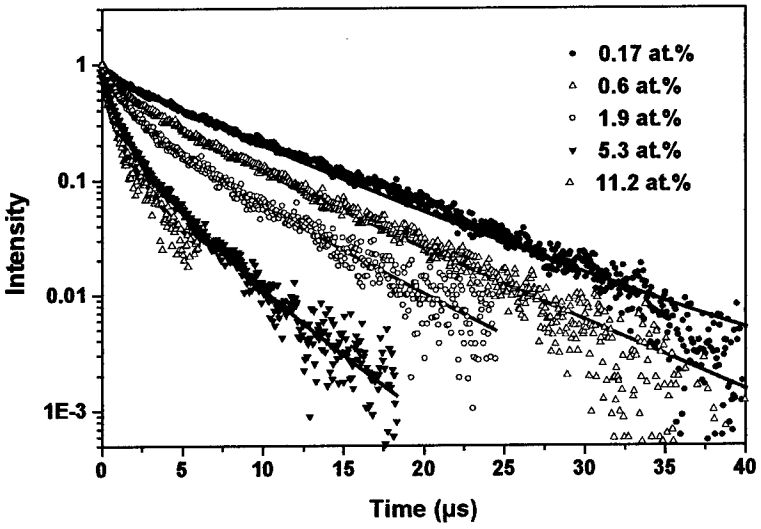

2.2. Infrared emission

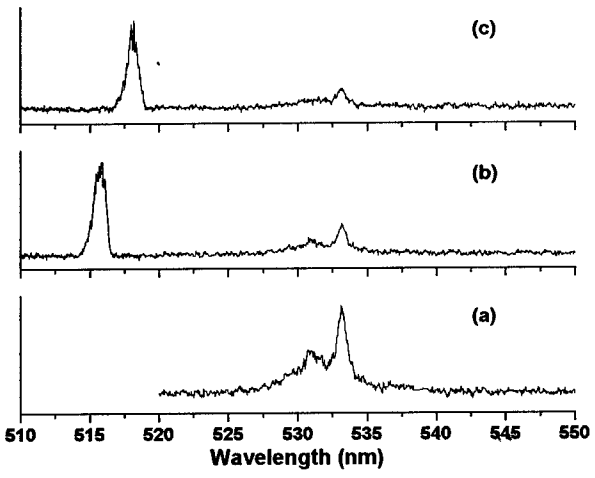

Figure 6a :Selective excitation spectrum of the $^4I_{13/2} \rightarrow {}^4I_{15/2}$ transition recorded at 10K for GaN:Er^{3+} (0.6 at.%)
(a : $\lambda_{analysis}$ = 1537 nm ;b : $\lambda_{analysis}$ = 1545nm ;c : $\lambda_{analysis}$= 1552 nm)

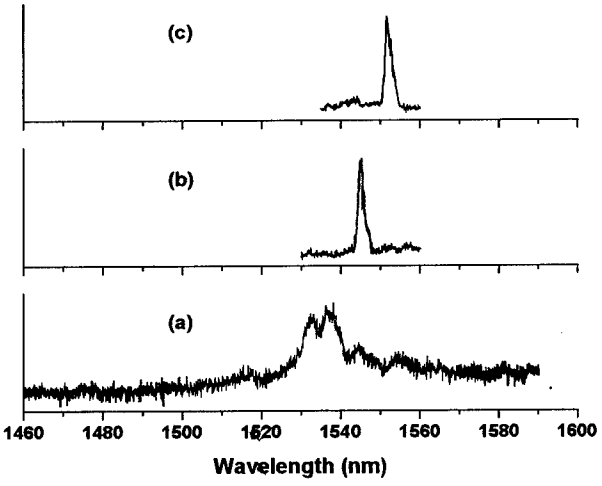

Figure 6b : $^4I_{13/2} \rightarrow {}^4I_{15/2}$ Fluorescence spectrum recorded at 10K for GaN :Er^{3+} (0.6 at.%) with selective excitation (a : $\lambda_{excitation}$ = 533.7 nm ; b : $\lambda_{excitation}$ = 515.7 nm ; c: $\lambda_{excitation}$ = 518 nm)

2.3. Time resolved emission spectrum for the C1 center

Figure 7: $^4I_{13/2} \rightarrow {}^4I_{15/2}$ Time resolved emission spectrum recorded at 10K with excitation in the $^2H_{11/2}$ (C1) multiplet.

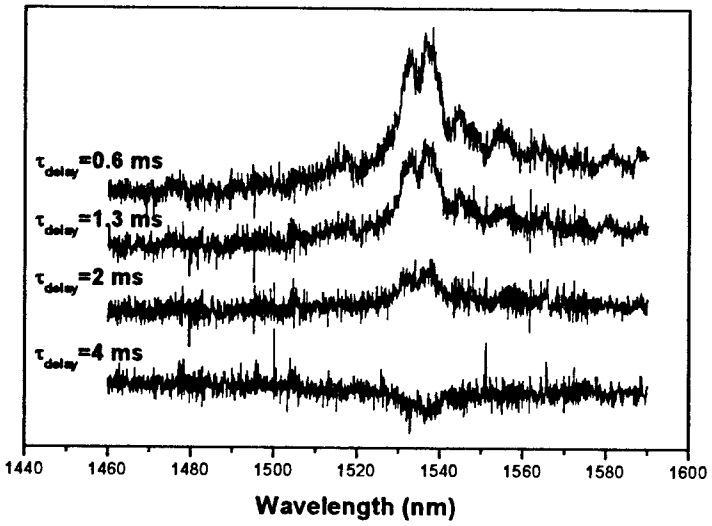

2.4. Decay time of the infrared emitting level

Figure 8 : $^4I_{13/2}$ decay profile as a function of excitation wavelength recorded at 10K (a : $\lambda_{excitation}$ = 533.7 nm and $\lambda_{analysis}$ = 1537 nm corresponding to C1 ; b : $\lambda_{excitation}$ = 515.7 nm and : $\lambda_{analysis}$ = 1545nm corresponding to C2 ; c : $\lambda_{excitation}$ = 518 nm and $\lambda_{analysis}$= 1552 nm corresponding to C3) (full line : theoretical fit ; cross : experimental curves).

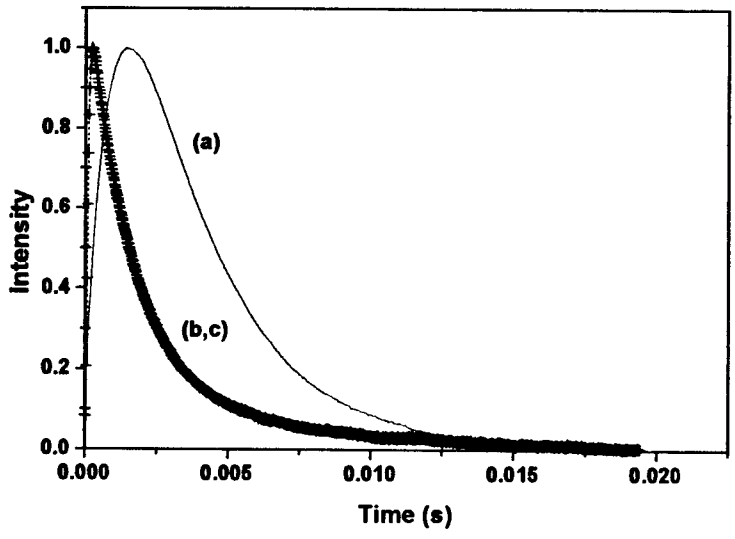

The temporal behavior of the luminescence intensity has been modeled using a simple model with a rise (τ_r) and exponential decay (τ_d):

$$\tau = C[\exp(-t/\tau_d) - \exp(-t/\tau_r)]$$

where C is a constant, tr and td. are the rise and decay time respectively. Best fit of the experimental curves were obtained with the parameters reported in tables I and II.

Table I : $^4I_{13/2}$ rise and decay times measured at 10K for the different centers (GaN: 0.6 at.% Er^{3+})

	$\lambda_{excitation}$ (nm)	Rise time (µs)	Decay time (ms)
C1	533.7	862	3.1
C2	515.7	64.5	1.718
C3	518	79	1.773

Table II: $^4I_{13/2}$ rise and decay times measured at room temperature as a function of Er^{3+} concentration ($\lambda_{excitation}$ = 533.7nm, analysis for center C1 at $\lambda_{analysis}$ = 1537nm).

[Er^{3+}] (at.%)	Rise time (µs)	Decay time (ms)
0.17	98	2.43
0.6	33.6	1.41
1.9	21	0.310

ANNEX B

Energy transfer

1. Theory : Diffusion limited model

In the frame of this model, two subset of ions interact : the sensitizers which are optically excited and the acceptors which trap the electronic excitation. The decay of the total sensitizer system results from the contribution of excited sensitizers lying nearby acceptors which predominantly relax by direct ion-pair energy transfer and the contribution of other more distant sensitizers which must first diffuse into the vicinity of an acceptor before relaxation occurs. In this case, the sensitizer luminescence intensity *I(t)* as a function of time is described by solving a diffusion equation.

For low acceptor concentrations, only a small fraction of the total number of excited sensitizers are within the critical distance of an acceptor and the sensitizer decay is then governed principally by intrinsic relaxation and by diffusion-limited relaxation to acceptors.

As the acceptor concentration increases, a larger fraction of the sensitizers are located within the critical interaction range of acceptors and energy migration becomes negligible. Yokota and Tanimoto have obtained a general solution for the sensitizer decay function including diffusion within the sensitizer system and sensitizer-acceptor energy transfer via a dipole-dipole coupling [1] :

$$I(t) = I(0)\exp\left[-\frac{t}{\tau_0} - \frac{4\pi}{3} N_A \left(\alpha_{SA} t\right)^{1/2} \left(\frac{1+10.87x+15.50x^2}{1+8.743x} \right)^{3/4} \right] \qquad [1]$$

where N_A is the acceptor concentration, $x = D\,\alpha_{SA}^{-1/3} t^{2/3}$, with D is the diffusion constant and α_{SA} is the sensitizer-acceptor transfer constant.

At the earlier times of the decay, the diffusion is negligible and Eq. [1] reduces to the case of direct relaxation – no diffusion, I(t) can be written in a simple form :

$$I(t) = I(0)\exp\left[-\frac{t}{\tau_0} - \gamma\, t^{1/2} \right] \qquad [2]$$

$$\text{with} \qquad \gamma = \frac{4\pi}{3}\Gamma\left(1-\frac{3}{s}\right) N_A\, R_0^3\, \tau_0^{-1/2} \qquad [3]$$

where s= 6 (since this model is valid for a dipole-dipole interaction), R_0 is the critical concentration and τ_0, the intrinsic lifetime of the sensitizer without acceptor.

When $t \to \infty$, Eq (1) reduces to an exponential function of time with a characteristic time :

$$\frac{1}{\tau_{exp}} = \frac{1}{\tau_0} + \frac{1}{\tau_D} \qquad [4]$$

where $1/\tau_0$ is the intrinsic decay rate and $1/\tau_D$, the decay rate due to diffusion. In case of a dipole-dipole interaction :

$$\frac{1}{\tau_D} = 8.6\, N_A\, \alpha_{SA}^{1/4}\, D^{3/4} \qquad [5]$$

The quenching rate $1/\tau_D$ is concentration dependent and can be written as :

---

[1] M. Yokota and O. Tanimoto, *J. Phys. Soc. Japan*, **22**, 779 (1967).

$$\frac{1}{\tau_D} = \frac{1}{\tau_{exp}} - \frac{1}{\tau_0} = KN_S N_A \qquad [6]$$

where N_S and N_A are the sensitizer and activator concentrations, K is a constant which can be written as :

$$K = 8\pi\left(\frac{R_0}{R}\right)^6 \frac{1}{\tau_0} \qquad [7]$$

where R is the distance between sensitizer ions. Since Er^{3+} ions act as sensitizer and acceptor, we can approximate to Eq. [6] to KN^2, then

$$K = \frac{9}{2\pi}\left(\frac{1}{N_0}\right)^2 \qquad [8]$$

with N_0 the critical concentration related to the critical transfer distance by $R_0=(3/4\pi N_0)^{1/3}$. Then Eq. [4] can be written in a simple form for the asymptotic decay as a function of the sensitizer concentration [2]:

$$\tau = \frac{\tau_0}{\left[1+\frac{9}{2\pi}\left(\frac{N}{N_0}\right)^2\right]} \qquad [9]$$

2. Visible emission : Determination of the microscopic parameters of the energy transfer

The dependence of $Ln(I(t))+t/\tau_0$ at the earlier times of the decay is a linear function of $t^{1/2}$ which allows to deduce for a dipole-dipole interaction. The asymptotic part of the decay follows a quadratic dependence with Er^{3+} concentration. This allows to conclude to a diffusion-limited process (the best fit of the experimental values is obtain with $K=7.2\times10^{-39}$ cm^6s^{-1}).

From Eq [5] and Eq. [9], it is possible to extract τ_0 and N_0 from the concentration dependence of the lifetime of the asymptotic part of the decay.

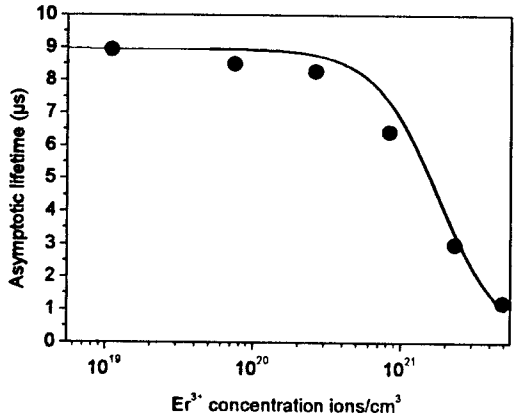

Figure 1 :Asymptotic decay rate of the $^4S_{3/2}$ temporal behavior as a function of Er^{3+} concentration (T=300K) (full line : theoretical fit using Eq [9] ; dots : experimental data).

---

[2] F. Auzel, F. Bonfigli, S. Gagliari and G. Baldacchini, *J. Lumin.*, **94-95**, 293 (2001).

The microscopic parameters are the following: $N_0 = 4.31 \times 10^{21}$ ions/cm^3 (4.84 at.%); $\tau_0 = 8.55$ µs ; $R_0 = 3.8$Å. The sensitizer-acceptor transfer constant α_{SA} is related to R_0 and τ_0 through the relation $\alpha_{SA}=R_0^6/\tau_0$, a value of 3.52×10^{-40} cm^6/sec is obtained for α_{SA}.

From the fit of the earlier part of the decay and values of N_A and R_0 we deduced the sensitizer-acceptor transfer rate W_{SA} using Eq.[5]. A constant value equal to 3.68×10^5 s^{-1} was obtained for the sensitizer-acceptor transfer rate in all the samples.

The initial part of the fluorescence transients depicted on Figure 5 (Annex1) was fitted using Eq. [2] with N_A as the only adjustable parameter. Fitting $I(t)$ using the complete expression Eq. [1] as derived by Yokota and Tanimoto is rather difficult. However, the diffusion constant can be calculated using Eq. [5]. The concentration dependence of the diffusion constant is depicted on Figure 2.

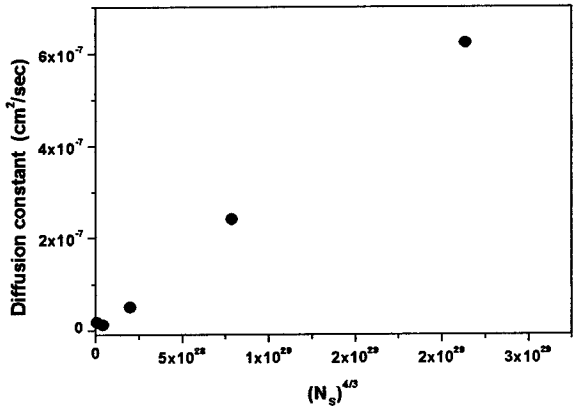

Figure 2: Diffusion constant as a function of sensitizer concentration. (dots: calculated values, full line: linear fit)

The asymptotic decay time $1/\tau_D$ plotted as a function of the sensitizer-sensitizer transfer rate expressed in units of the trapping rate in Log-Log scale (Figure 3) exhibits a linear dependence between 0.6 and 11.2 at.%, with a slope (equal to 0.6) less than unity which confirms the validity of using the diffusion limited model in this concentration range.

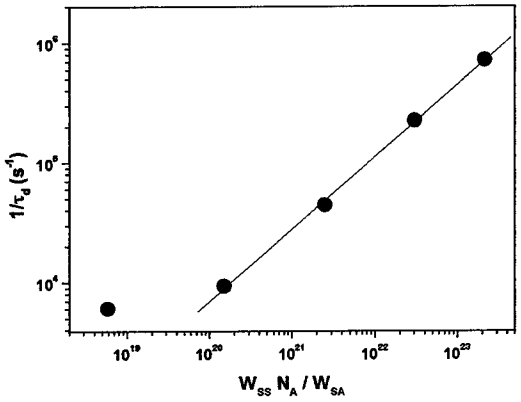

Figure 3: Asymptotic decay rate as a function of the trapping rate in a log-log plot ($W_{SS}N_A/W_{SA}$) (full line : linear fit ; dots : experimental data).

3. Quenching of the infrared emission

The quenching behavior of the $^4I_{13/2}$ state is still well described by a limited diffusion process as shown by the simulation by Eq.[9] as shown on Figure 4. The corresponding τ_0 is found to be 2.48ms, and the critical concentration is $N_0 = 0.67.10^{21}$ cm^{-3} (0.8 at.%).

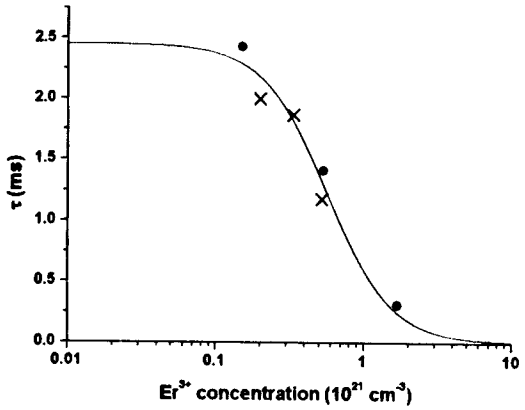

Figure 4: Self-quenching of $^4I_{13/2}$ and the limited diffusion hypothesis. Continuous curve is simulation by Eq. [9] with parameters: τ_0=2.45 ms; N_0=0.67 $10^{21}cm^{-3}$; points marked as X, are for samples prepared with an increased N content.

ANNEX C

Crystal field strength analysis

1. Crystal field parameter :Theory

From the overall splitting of the $4f^N$ multiplets field, it is possible to deduce the crystal field strength using a scalar field parameter.

The crystal state energies are given by the eigenvalues of the matrix $\langle 4f^N SLJJ_z | V | 4f^N S'L'J'J'_z \rangle$, where V is the crystal field potential expressed as a function of the crystal field B_q^κ parameters following :

$$V = \sum_{k\neq 0,q,i} B_q^k \left(C_q^k\right)_i \qquad [1]$$

For rare earth ions, k=2,4,6 and q has $2q$+1 values such that $|q| < k$. For low site symmetry, 15 different B_q^κ parameters are needed to describe the crystal field effect on the Stark levels. This precludes a simple comparison of the crystal field strength between several hosts. The scalar crystal field parameter N_v was introduced to allow a simple comparison between different host materials. N_v is simply expressed as :

$$N_v = \left[\sum_{k\neq 0 q} \frac{4\pi}{2k+1} \left(B_q^k\right)^2 \right]^{1/2} \qquad [2]$$

The maximum splitting $\Delta E(J)$ for a J given state of a rare earth ion in a crystal is then simply related to N_v following :

$$\Delta E(J) = K^{1/2} \left[\prod_{k=2,4,6} \left| \langle J \| C^k \| J \rangle \right| \right]^{1/3} N_v \qquad [3]$$

with $$K = \frac{3g_a{}^2}{g(g_a+2)(g_a+1)\pi}$$

and g_a being the degeneracy effectively removed by the crystal field, g_a=$g/2$ for J half integer. The matrix elements are easily calculated using :

$$\langle J \| C^k \| J \rangle^2 = \langle f \| C^k \| f \rangle^2 \langle [SLJ] \| U^k \| [SLJ] \rangle^2 \qquad [4]$$

Square roots of the first matrix elements are respectively equal to –1.36, 1.13 and –1.27 for k=2,4,6 respectively, the second reduced matrix elements have been calculated by Carnall et al [1].

---

[1] W.T. Carnall, H. Crosswhite and H.M. Crosswhite, *Energy levels structure and transition probabilities of travalent lanthanides in LaF_3*, Argonne National Laboratory, Argonne I11, 4493 USA (1977).

2. Crystal field strength in GaN

Eq. [3] gives the following expressions for the multiplets of interest in this work :

$$\Delta E(15/2) = 0.192\ N_V \quad [5a]$$

$$\Delta E(13/2) = 0.117\ N_V \quad [5b]$$

The overall splittings, measured for the $^4I_{15/2}$ ground multiplet and calculated using Eq.[5b] for the first excited $^4I_{13/2}$ multiplet, are reported in Figure 1 in comparison with the experimental values found in literature for several inorganic materials.

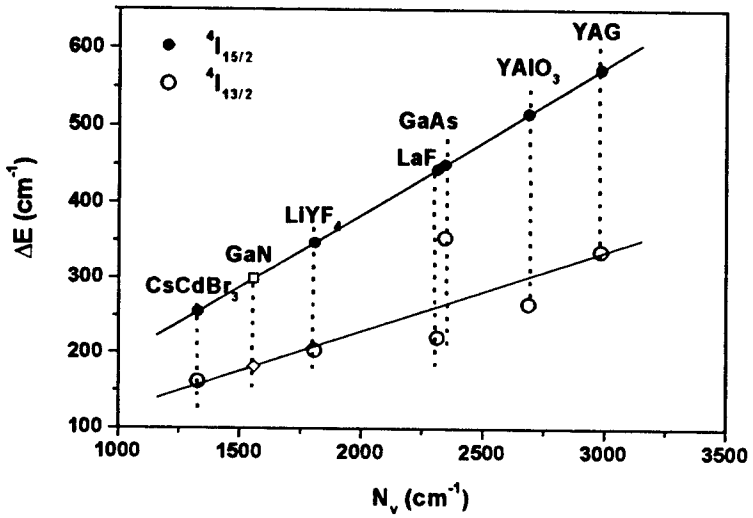

Figure 1: The overall splitting of the $^4I_{15/2}$ and $^4I_{13/2}$ multiplets for several Er^{3+} doped inorganic materials corresponding to different structures and site symmetries. Full lines correspond to Eq. [5a] and Eq. [5b]. Dots (full and open) correspond to the experimental values reported in literature.

3. Nephelauxetic effect

The nephelauxetic effect is linked with the nature of the bounding between the rare earth and the ligands. In case of covalent bounding, the transitions are shifted toward the red. The $^4I_{13/2}$-$^4I_{15/2}$ transition barycenter at 1.5 μm for various Er^{3+} doped hosts calculated from the experimental results given in literature are gathered in Table 1 in comparison with that obtained in GaN.

The barycenter value found for GaN is between the value for YAG and $CsCdBr_3$ and clearly shows a covalent surrounding. the corresponding results are summarized in Figure 2.

Table III The $^4I_{13/2}$-$^4I_{15/2}$ transition barycenter for various Er^{3+} doped hosts

Host	LaF_3	$LiYF_4$	$YalO_3$	GaAs	YAG	GaN	$CsCdBr_3$
Barycenter (cm^{-1})	6479	6477	6469	6468 (O center)	6465	6462	6449
Anion	F	F	O	O	O	N	Br
χ (Pauling)	3.9	3.9	3.5	3.5	3.5	3	2.8

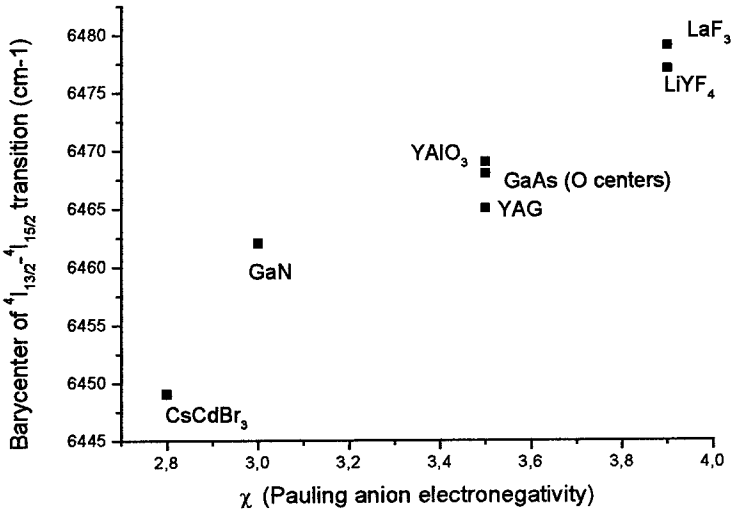

Figure 2: The $^4I_{13/2}$- $^4I_{15/2}$ transition barycenters for selected Er^{3+} doped hosts.

ANNEX D

Spetroscopy of Eu^{3+}:GaN

Table 1. Number and symmetry labels of the c.f. components of the ^7F_J (J=0-3) levels for the C_{3v} site symmetry.

	C_{3v}		
J	A_1	A_2	E
0	1		
1		1	1
2	1		2
3	1	2	2

Table 2. Selection rules of multipole transitions for the C_{3v} site symmetry.

	C_{3v}					
	Electric dipole			Magnetic dipole		
	A_1	A_2	E	A_1	A_2	E
A_1	π		σ		π	σ
A_2		π	σ	π		σ
E	σ	σ	π	σ	σ	π

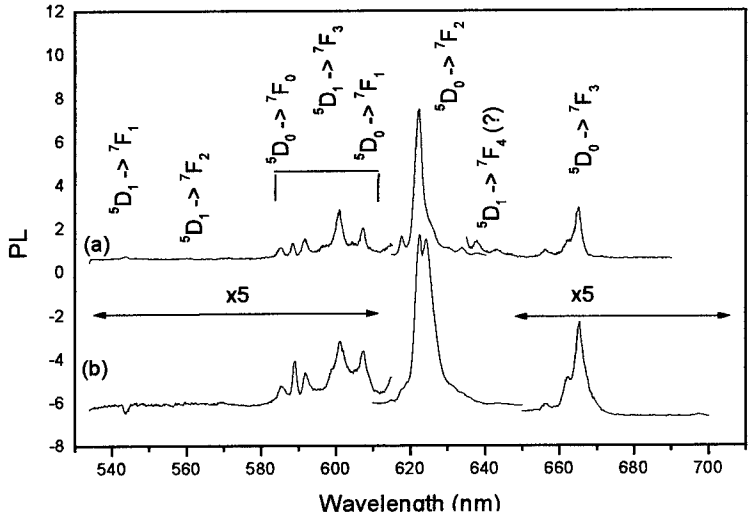

Figure 1: Emission of Eu^{3+}:GaN at room temperature with excitation above the energy band gap (λ=355 nm; a-D120, b-D035)

)

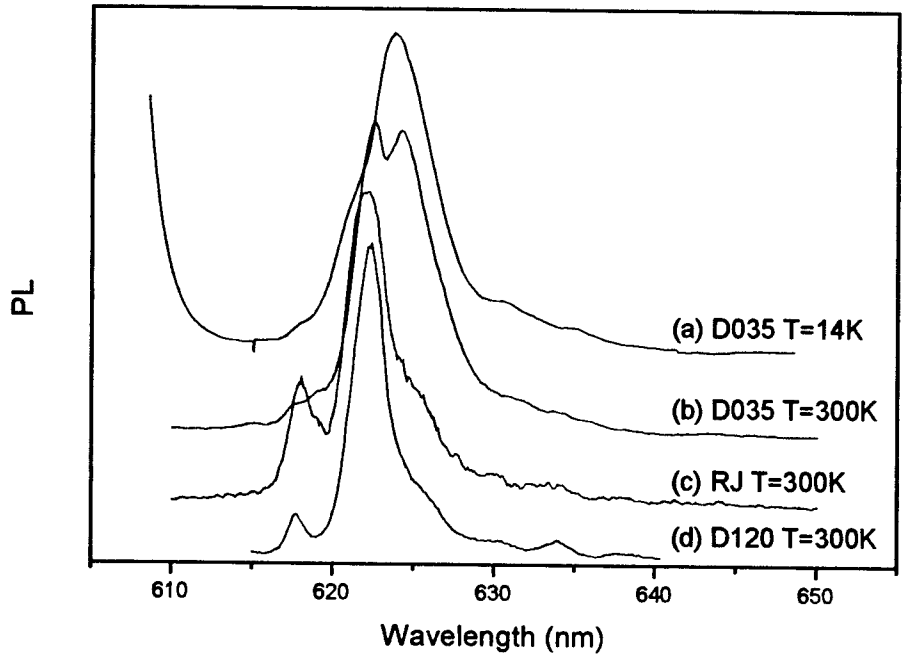

Figure 2: $^5D_0 \rightarrow {}^7F_2$ transition recorded for the different Eu^{3+}:GaN samples (λ_{exc}=355 nm, T=300 K)

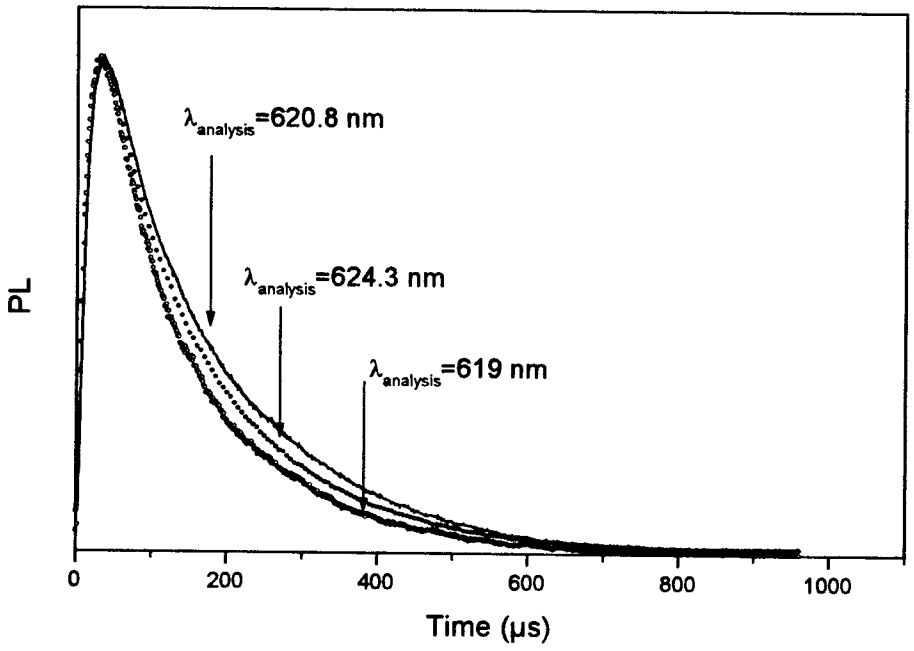

Figure 3: $^5D_0$ decay profiles measured at several wavelengths for the Eu^{3+}:GaN sample D035 excited at λ_{exc}=355 nm, T=300 K

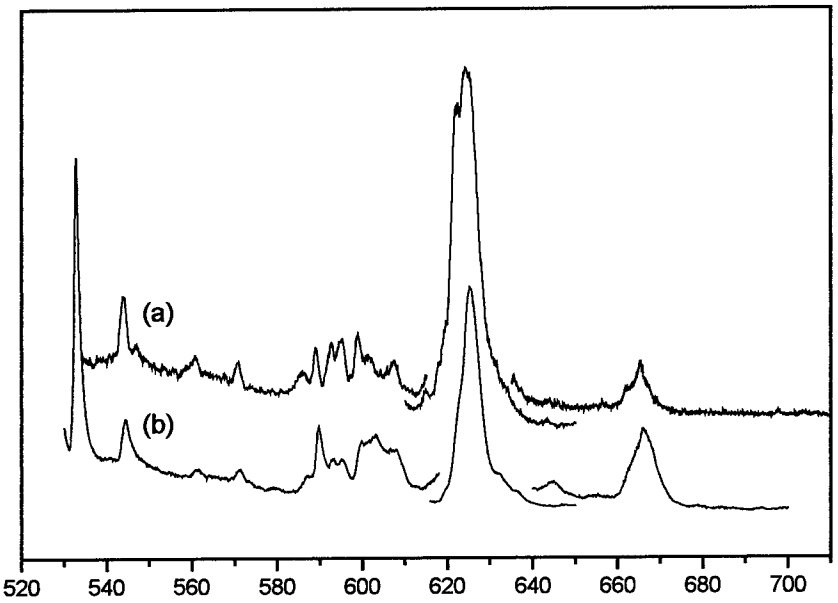

Figure 4: Luminescence spectrum recorded for the Eu^{3+}:GaN sampleD035 under excitation above the energy band gap (a- T=300 K, b- T=10 K)

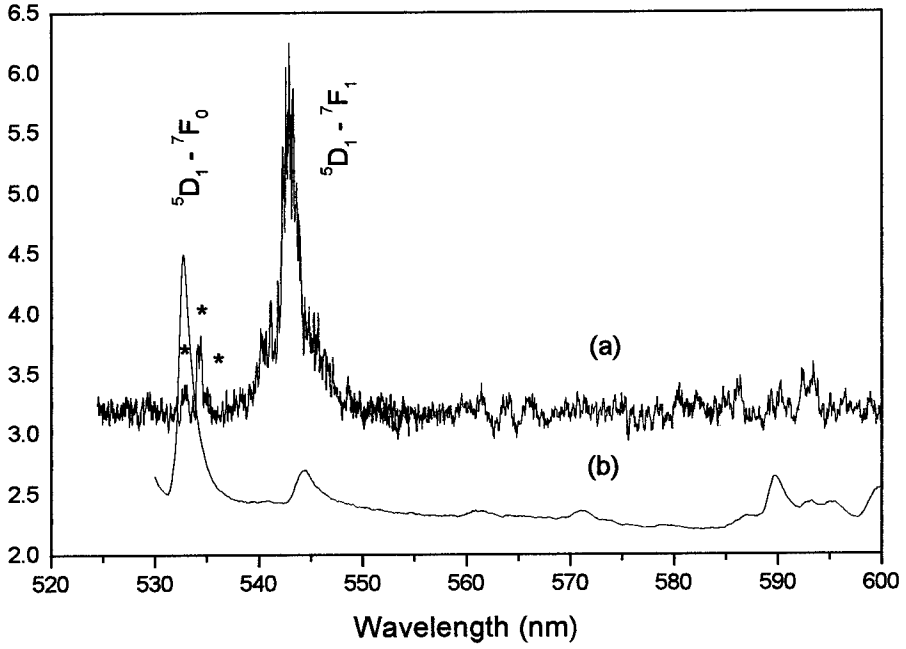

Figure 5: a- Excitation spectrum recorded at room temperature monitoring $^5D_0 \rightarrow {}^7F_2$ at 622 nm (D035).
b- Emission spectrum recorded at low temperature (T=10 K, λ_{exc}=355 nm)

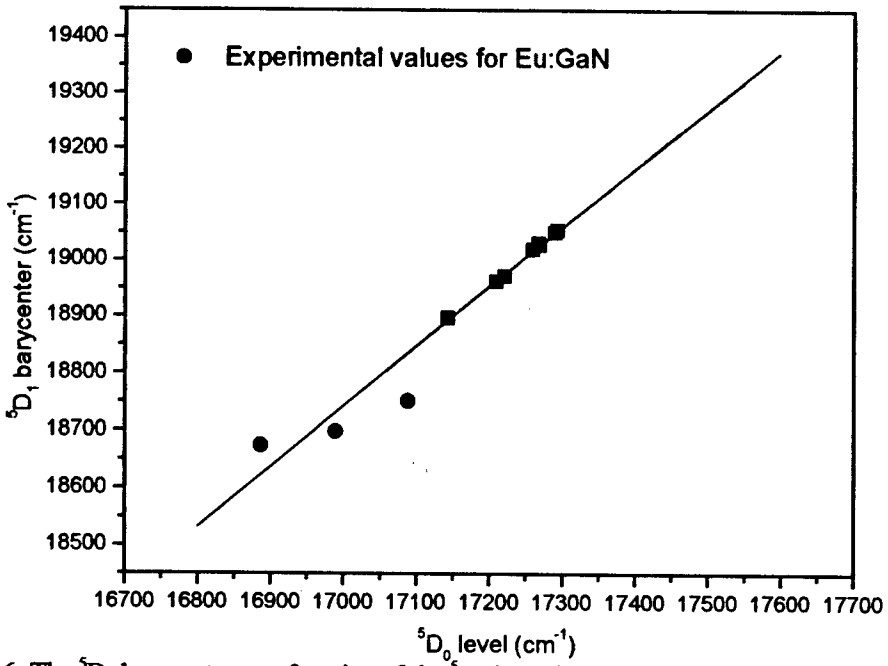

Figure 6: The $^5D_1$ barycenter as a function of the $^5D_0$ level for different crystalline compounds (by courtesy of Dr. E. Antic Fidancev)

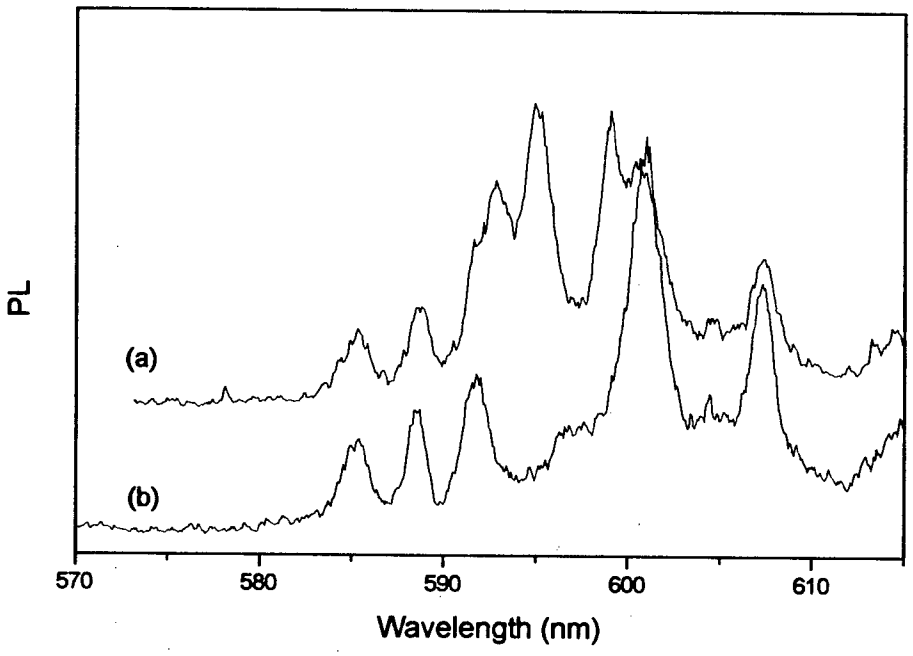

Figure 7: Time resolved luminescence spectra of Eu^{3+}:GaN (T=300 K, λ_{exc}=355 nm)
- a- spectrum recorded 5 μs after the excitation pulse
- b- spectrum recorded 100 μs after the excitation pulse

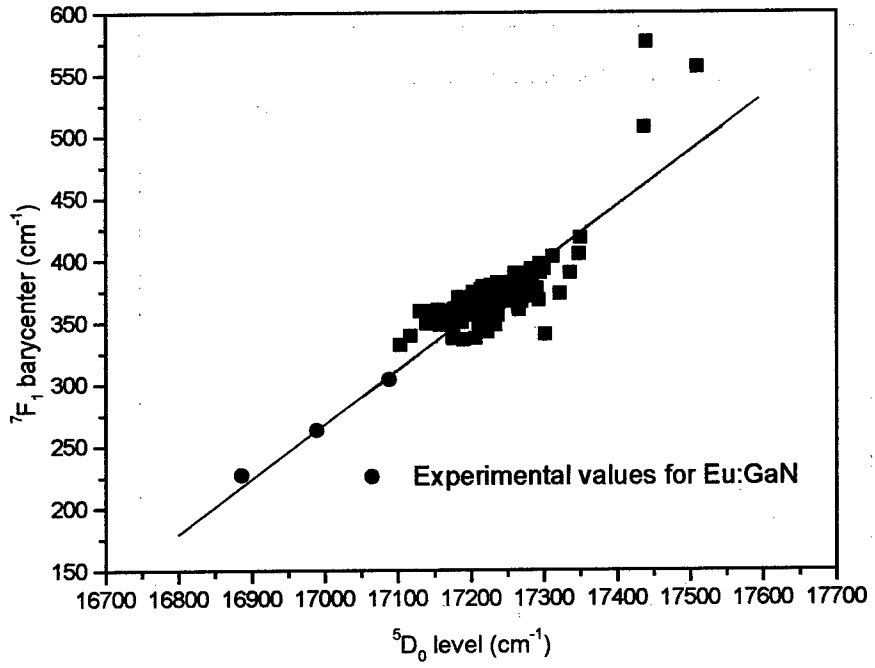

Figure 8: The $^7F_1$ barycenter energy as a function of the $^5D_0$ level energy for different crystalline compounds (by courtesy of Dr. E. Antic Fidancev)

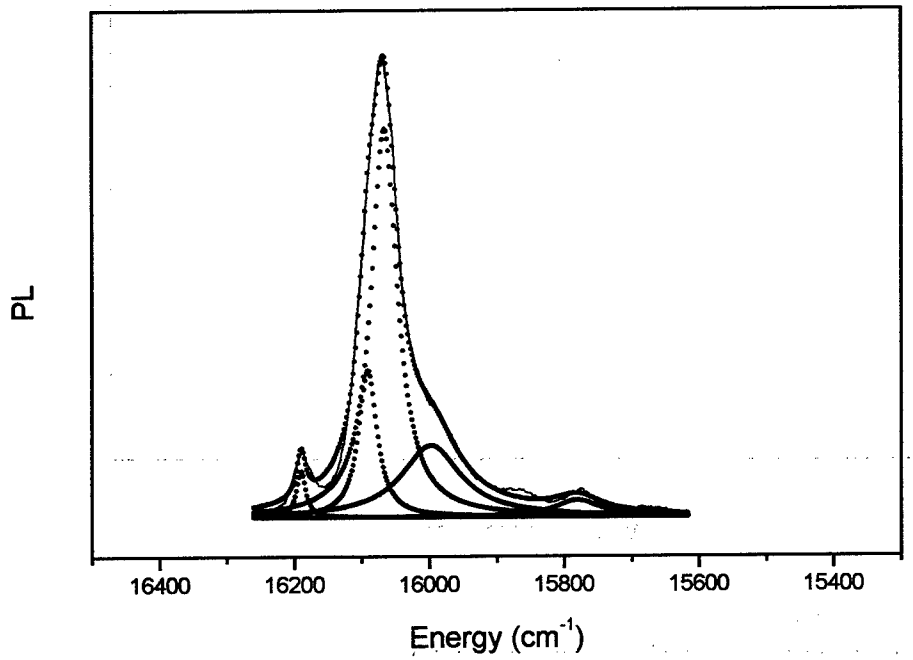

Figure 9a: Deconvolution of the $^5D_0 \rightarrow {}^7F_2$ transition for the Eu^{3+}:GaN sample D120 excited at 355 nm at room temperature (dotted lines: calculated curves)

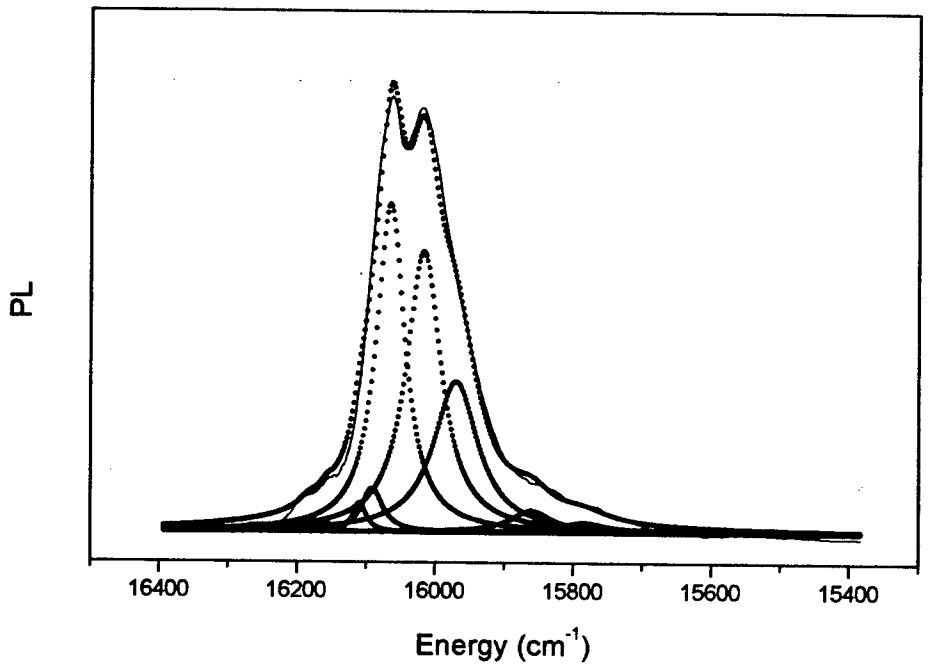

Figure 9b: Deconvolution of the $^5D_0 \rightarrow {}^7F_2$ transition for the Eu^{3+}:GaN sample D035 excited at 355 nm at room temperature (dotted lines : calculated curves)

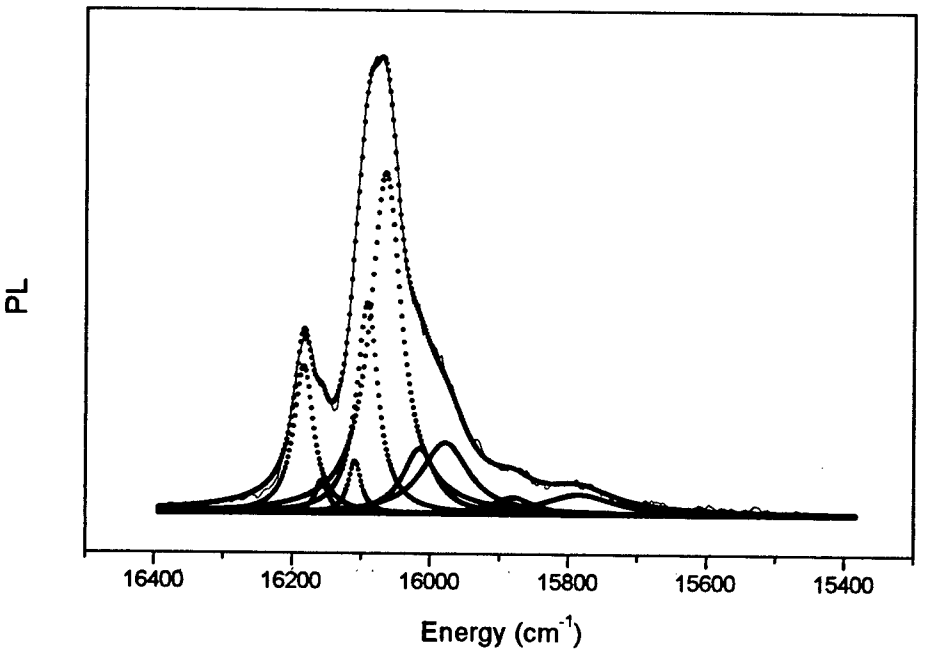

Figure 9c: Deconvolution of the $^5D_0 \rightarrow {}^7F_2$ transition for the Eu^{3+}:GaN sample RJ_081 excited at 355 nm at room temperature (dotted lines : calculated curves)

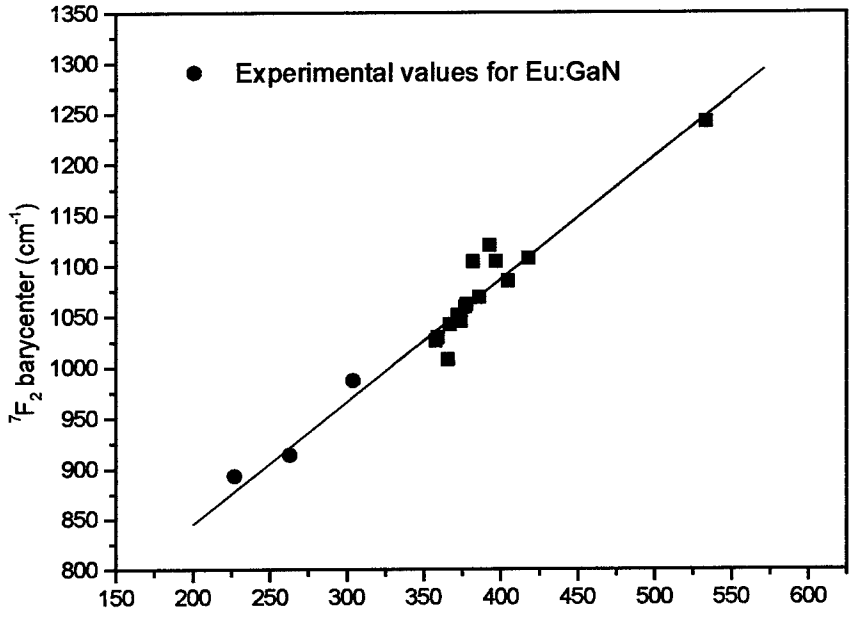

Figure 10: The $^7F_2$ barycenter energy as a function of the $^7F_1$ barycenter energy for different crystalline compounds (by courtesy of Dr. E. Antic Fidancev)

$^{2S+1}L_J$	C1	C2	C3
$^5D_1$	18751	18698	18674
$^5D_0$	17088	16989	16886
$^7F_0$	0	0	0
$^7F_1$ E	335	221	130
$^7F_1$ A	243	349	421
$^7F_1$,bc	**304**	**263**	**227**
$^7F_2$ E	933	806	778
$^7F_2$ E	995	924	912
$^7F_2$ A	1078	1109	1088
$^7F_2$,bc	**987**	**914**	**894**

Table 4: Experimental energies and irreducible representation of the $^{2S+1}L_J$ crystal field components for Eu^{3+}:GaN in the C_{3v} point symmetry

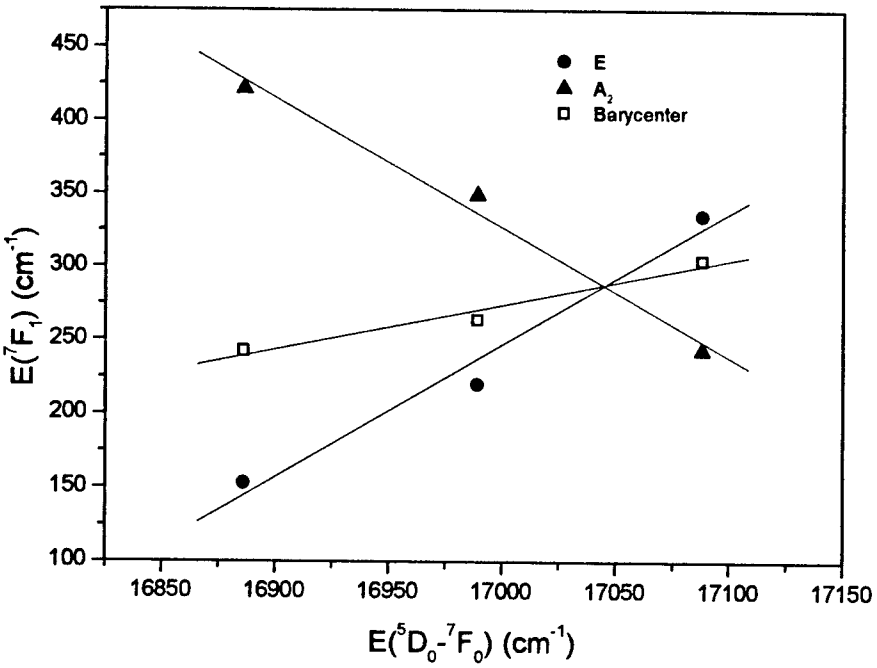

Figure 11: Energy of the crystal field components and barycenter of $^7F_1$ for the different centers in Eu^{3+}:GaN

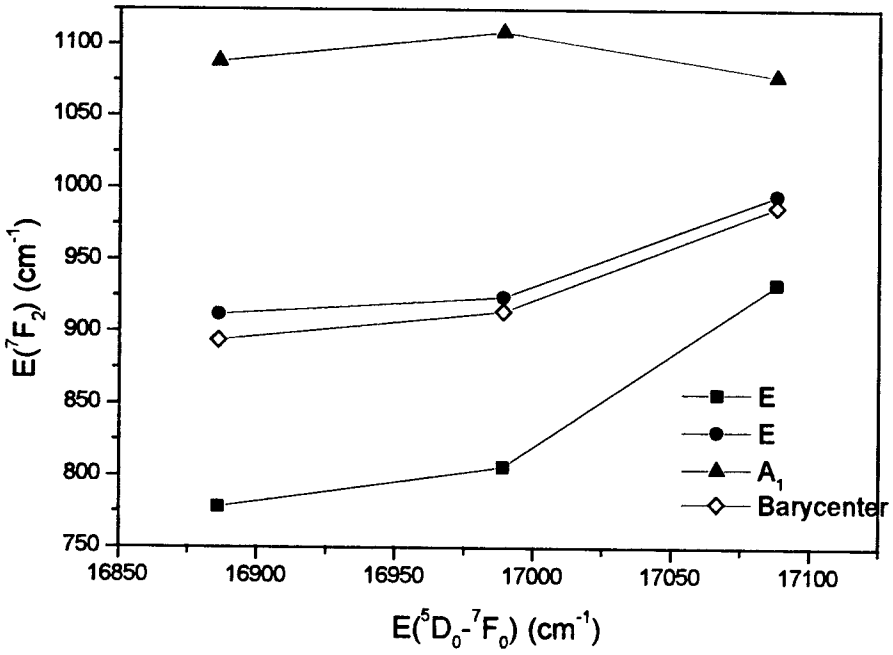

Figure 12: Energy of the crystal field components and barycenter of $^7F_1$ for the different centers in Eu^{3+}:GaN

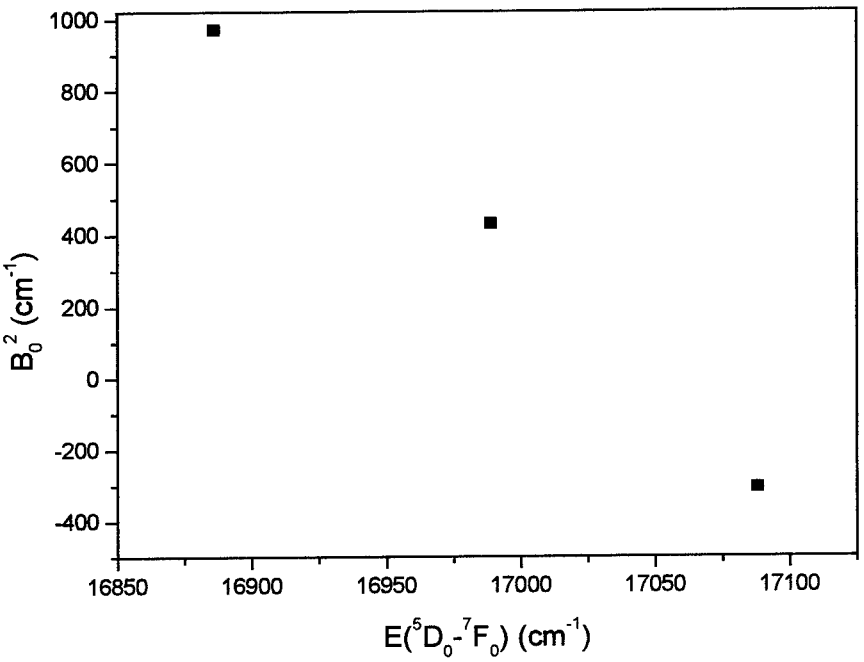

Figure 13: The calculated crystal field parameter B_0^2 for the different centers in Eu^{3+}:GaN

Annex E

Conferences and Publications

- Invited conference given by F. Pellé at ICPCL2002 (International Conference on Physics of Laser Crystals - Ukraine august 2002)

Fluorescence dynamics of Er^{3+} ions in MBE-grown GaN-thin films

F. Pellé, F. Auzel, J.M. Zavada, A.J. Steckl

- Publication to be published in NATO SCIENCES SERIES VOLUME : Physics of laser Crystals

Fluorescence dynamics of Er^{3+} ions in MBE-grown GaN-thin films

F. Pellé, F. Auzel, J.M. Zavada, A.J. Steckl

- Oral presentation at the Electrochemical Society, 203 rd Meeting, Paris, April 27- May 2, 2003

New spectroscopic data of erbium ions in GaN thin films

F. Pellé, F. Auzel, J.M. Zavada, A.J. Steckl

- Publication submitted at the Journal Electrochemical Society

New spectroscopic data of erbium ions in GaN thin films

F. Pellé, F. Auzel, J.M. Zavada, D.S. Lee, A.J. Steckl

- Oral presentation at the Workshop on "Impurity based Electroluminescence in Wide Bandgap Semiconductors" Santa F, New Mexico, April 13-16, 2003

Site-Selective Excitation Spectroscopy of Er- doped GaN

F. Pellé, F. Auzel, J.M. Zavada, D.S. Lee and A.J. Steckl

- Oral presentation accepted at the European Material Conference (E-MRS 2003 Spring Meeting) Strasbourg June 10-13, 2003

Site-Selective Excitation Spectroscopy of Er- doped GaN

F. Pellé, F. Auzel, J.M. Zavada, D.S. Lee and A.J. Steckl